VENTILATION AND RADON DYNAMICS IN MAINE SEASONAL SNOWCOVER

Daniel J. Breton*
Department of Physics and Astronomy, University of Maine, Orono, Maine

ABSTRACT: Radon concentrations and fluxes were measured for seasonal snowpack on Baldpate Mtn. in Newry, Maine during the winter of 2004. A solar radiation and temperature logging system was developed to monitor the snowpack during the radon measurements.
Radon ground flux measurements were performed using a RAD-7 alpha spectrometer and ranged from 0.49 to 0.64 pCi m^{-2} s^{-1} for two different locations. Radon concentration as a function of time was measured inside the snowpack using a Honeywell A9000 radon monitor and showed average radon concentrations ranging from 1 to 12 pCi L^{-1}, though maximum concentrations of over 80 pCi L^{-1} were observed.
Wind-driven and natural circulation airflows within the snowpack were shown to be the major factors controlling radon dynamics. Dilution rates of 1.25 pCi L^{-1} h^{-1} were correlated with windspeeds of 9 m s^{-1}, while radon concentration rates of 0.8 pCi L^{-1} h^{-1} were observed during periods of calm. Comparison of long term track-etch cup measurements with radon diffusion theory showed that radon within the snowpack rarely exists in steady state distribution due to the ventilation effects of wind and natural circulation air flows. This study shows that radon dynamics can be used to measure air flows inside the snowpack.

KEYWORDS: ventilation, radon, wind-driven circulation, natural circulation

1 INTRODUCTION

New England is a region which contains rugged, low lying mountains, seasonal snowfall and many areas with high radon concentrations measured in homes and groundwater. This combination of qualities provides an excellent opportunity to study the upward flux of natural radioactivity into a seasonal snowpack from the ground.

Work on the distribution and diffusion of radon in soil has been ongoing for many years in order to help understand influx rates into homes and public buildings(Kraner et al., 1964), (Tanner, 1964), (Lockhart, 1964). The shielding effect of snow for naturally occurring terrestrial gamma radiation has been exploited by the National Operational Hydrologic Remote Sensing Center to estimate snow depths by using aircraft-mounted gamma detectors(Carroll, 2001). However, no study has been conducted on the actual behavior and distribution of radon activity within the snow.

This study was conducted to assess the amount of radon present in the snow, the magnitude of the radon flux from the soil in various winter conditions, and the effects of air movement through the snowpack on the observed radon distribution. We hypothesize that radon and its daughters can be used as a tracer gas to study environmental and metamorphic changes in a seasonal snowpack.

We pose three specific questions to expand on the hypothesis posed above:

1. Is ^{222}Rn movement driven by heat fluxes and does it therefore migrate with water vapor within the snowpack? Could it be used as a tracer gas to monitor water vapor movement?
2. Does meltwater formation in the upper layers of the snowpack effectively "seal" the surface of the snow, thus preventing the escape of ^{222}Rn from the snow?
3. Are wind-driven and natural circulation air flows significant in terms of their diluting effect on the ^{222}Rn concentration within the snowpack?

The sections that follow describe the theoretical models and experimental techniques used in this study to attempt to answer these questions.

2 THEORY

Beginning with the source of radon itself, the discussion follows its departure from the ground and its upward journey through the snowpack. Along the way, it may encounter changes in porosity, obstacles such as ice layers or meltwater and be subject to dilution by ambient air intrusion into the snowpack. Concluding this section, wind-driven and natural circulation flows of ambient air into the snowpack are discussed.

2.1 *Production of ^{222}Rn from geological sources*

^{222}Rn is part of the uranium decay series, which begins with naturally existing ^{238}U in the earths crust and ends with ^{206}Pb. We begin with the immediate precursor of ^{222}Rn, ^{226}Ra with a half-life of 1622 y and transforming via alpha decay(Baum et al., 2002). ^{226}Ra

*Corresponding author address: Daniel Breton, 13010 SE Salmon Street, Portland OR 97233; email: dan@debroglie.umephy.maine.edu

is observed in almost any terrestrial sample, however certain granitic and high-grade metamorphic bedrock types are strongly correlated with elevated radon production rates, which implies an elevated ^{226}Ra content.(Gunderson, 1993)

^{222}Rn, with a 3.825 d half-life, is a noble gas and therefore is highly mobile and immediately begins migrating towards regions of lower radon concentration.(Cember, 1992) Radon and its daughters undergo a chain of decays which result in the release of three alpha particles and two betas before reaching the long lived ^{210}Pb, shown in Table 1. Most radon measurement instrumentation utilizes the strong ionizing effect of the alpha particles to determine the amount present.

Table 1: Portion of the radon decay chain

Isotope	$t_{1/2}$	Decay mode	Phase
^{222}Rn	3.78 d	α	Gas
^{218}Po	3.10 m	α, γ	Solid
^{214}Pb	27.0 m	β^-, γ	Solid
^{214}Bi	19.9 m	β^-, γ	Solid
^{214}Po	164 μs	α	Solid
^{210}Pb	22.3 y	β^-, γ	Solid

2.2 *Theoretical basis for measurement of ^{222}Rn ground flux*

The ground flux of ^{222}Rn, Φ_g, is measured in atoms m^{-2} s^{-1} and represents the total radon exhalation rate per unit area for a given location. If this exhalation rate is uniform over the area to be measured, then we can determine Φ_g by enclosing this area with a known, airtight measurement volume and monitoring the radon concentration as a function of time within the volume. Any real radon detector used to do the monitoring will have a finite volume of its own, $V_{\text{instrument}}$ which must be accounted for.

For a container with a height h and an opening of area A covering soil with a ground flux Φ_g, the change in radon concentration C per unit time is

$$\begin{aligned}\frac{\Delta C}{\Delta t} &= \frac{\text{Rate of activity entering measurement volume}}{\text{Total volume}} \\ &= \frac{\Phi_g A}{(hA)\pm(V_{\text{instrument}})}\end{aligned} \tag{1}$$

where we add the air volume of the instrument if it is external to the measurement volume and subtract it if it is located inside the measurement volume. The RAD-7 instrument used in this study is located outside the flux measurement volume.

We can use the concentration rate data and the dimensions of the airtight volume to solve this equation for an average value of Φ_g during time Δt:

$$\begin{aligned}\Phi_g &= \left[\frac{\Delta C}{\Delta t}\right] \frac{(hA)\pm(V_{\text{instrument}})}{A} \\ &= \left[\frac{\Delta AC}{\Delta t}\right] \frac{(hA)\pm(V_{\text{instrument}})}{A\lambda}\end{aligned} \tag{2}$$

where AC is the activity concentration, reported in pCi m^{-3} or similar units. Since radon detectors only measure the radon activity, the AC definition for the ground flux is the one used in practice.

2.3 *Radon diffusion in a porous medium*

Radon from the ground flux will diffuse through porous snow and eventually migrate out of the snow into the ambient air. This diffusion transport is driven by a concentration gradient existing between the snow/ground interface and the ambient air. The governing equations are partial differential equations which describe the fluxes and concentration rates of the substance as a function of time and space. The general expression for the flux J is

$$J = -D\nabla N \tag{3}$$

and the concentration rate at a given location is given as

$$\frac{\partial N}{\partial t} = D\nabla^2 N \tag{4}$$

where D is the diffusion coefficient for the substance in a particular medium and N is a function of space and time defining the distribution of the substance.(Boas, 1983) In this case, N is the number of radon atoms contained within a differential volume of air.

Now, we must adapt these equations for the diffusion of radon activity in porous snow and define the boundary conditions. The diffusion equation is shown in Eq. 5. The one-dimensional diffusion equation for radon in snow with constant porosity ϕ is

$$\frac{\partial N}{\partial t} = \begin{cases} (D_0\phi^3)\frac{\partial^2 N}{\partial z^2} - N\lambda & \text{for } z \geq 0 \\ (D_0\phi^3)\frac{\partial^2 N}{\partial z^2} - N\lambda + \Phi_g A & \text{for } z = d \end{cases} \tag{5}$$

Each term in this equation has the units of radon atoms s^{-1}, representing the gain and loss rates for radon within a differential volume.

The term $N\lambda$ accounts for the radioactive decay rate of radon.(Kraner et al., 1964) The effect of the snow porosity ϕ is incorporated into the diffusion coefficient as $D = D_0\phi^\chi$ where D_0 is the diffusion coefficient of radon in air and χ is an experimentally determined number. Based on SF_6 diffusion measurements made in Greenland snows, we will use $\chi = 3$ for this study.(Albert and Shultz, 2002)

The two boundary conditions consist of a radon concentration of N_∞ at the snow surface $z = 0$ where it is open to the ambient air, and a constant input flux Φ_g condition at the snow-ground interface $z = d$. If we assume a uniform Φ_g over a large extent of flat ground, diffusion will only occur only in the $-z$ direction shown in Fig. 1. Since ϕ is not necessarily a constant with re-

Figure 1: Schematic of radon diffusion geometry.

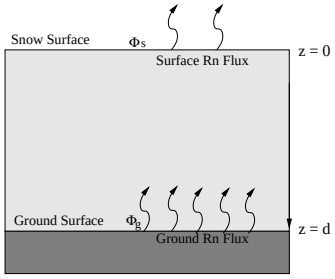

spect to time or position we must use a numerical solution to these diffusion equations. This will allow for the diffusion analysis to be applied to the actual conditions measured during this study. One of the most straightforward techniques for solving the diffusion equation, and the one used here, is the finite-difference method which discretizes both space and time variables into nodes and timesteps respectively(Incropera, 1996). By assigning the initial distributions of N and ϕ and using the finite-difference procedure, we can solve for $N(z)$ and $J(z)$ at any subsequent time. This calculation was implemented in the code `rndiff2.c`, available from the author.

2.4 *Meltwater generation and migration in seasonal snowpack*

The transport of radon in snow could be influenced by the presence of meltwater within the porespace of the snow. The melting of a snowpack is primarily controlled by the energy balance of the upper 50 cm of the snowpack, including solar and long-wave radiations, convection heat transfer with the ambient air and the energy added by precipitation. The interplay of these factors and the subsequent gravity-driven flow of meltwater within the snowpack is modeled in detail by the one-dimensional heat-transfer code `SNTHERM.89`, a FORTRAN code written by Rachel Jordan of the Cold Region Research and Engineering Laboratory(Jordan, 1991). This code performs an energy balance on the entire snow cover using meteorological data and snow parameters as inputs.

`SNTHERM.89` was used in this study to model the buildup and subsequent reduction in snow porosity due to meltwater blockage of porespaces in the upper layer of the snowpack during days of intense snowmelt. A change in the snow porosity directly affects the diffusion characteristics of radon through the snow since the diffusion coefficient of radon through water is over 6 orders of magnitude smaller than through air.

2.5 *Radon dilution*

Radon concentrations within the snow can be diluted by the flow of radon-free ambient air into the snowpack. Analyzing a given volume V of snowpack which covers an area A with depth of snow d, we can write an equation which describes the amount of radon N within this volume as a function of time:

$$\begin{aligned}\tfrac{\mathrm{d}N}{\mathrm{d}t} &= [\text{Input Rate}] - [\text{Loss Rate}] \\ &= [\Phi_g A] - [(\Phi_s A) + (N\dot{V}_t/Ad)] \end{aligned} \quad (6)$$

Here $\Phi_g A$ represents the input rate of radon from the ground area A beneath the snow, $\Phi_s A$ is the loss rate of radon through the snow surface and $(N\dot{V}_t/Ad)$ is the loss rate of radon due to dilution by a total flowrate $\dot{V}_t$ of radon-free air through the snowpack. $\dot{V}_t$ can consist of both wind-driven and natural circulation flows, discussed in Sections 2.6 and 2.7.

Calculating a net flux as $\Phi_{\mathrm{net}} = \Phi_g - \Phi_s$ and a ventilation constant as $T = \dot{V}/Ad$, we can rearrange Eq. 6 into a more standard form:

$$\frac{\mathrm{d}N}{\mathrm{d}t} + NT = \Phi_{\mathrm{net}} A \quad (7)$$

Since this is a first-order linear differential equation, we solve for $N(t)$ using an integrating factor and the initial condition that $N(0) = N_0$. Applying this technique, we find a general solution for $N(t)$:

$$N(t) = \frac{\Phi_{\mathrm{net}} A}{T}\left[1 - e^{-Tt}\right] + N_0 e^{-Tt} \quad (8)$$

It is useful to determine the value $\dot{V}_{\mathrm{critical}}$ which just balances the input and dilution rates of radon within the volume. In this state, the system will maintain a constant concentration with time. Taking the derivative of Eqn. 8 and applying the constant concentration condition $\frac{dN}{dt} = 0$, we obtain

$$\frac{\mathrm{d}N}{\mathrm{d}t} = 0 = \Phi_{\mathrm{net}} A e^{-Tt} - N_0 T e^{-Tt} \quad (9)$$

Solving this equation for $\dot{V}_{\mathrm{critical}}$, the flowrate which yields a constant concentration,

$$\dot{V}_{\mathrm{critical}} = \frac{\Phi_{\mathrm{net}} A^2 d}{N_0} \quad (10)$$

Therefore, maintaining a steady state concentration not only depends on the ground flux and volume, but is also inversely proportional to the initial concentration. This is an especially important result for correctly interpreting the data reported in Section 4.2.

This solution is unrealistic in that it assumes perfect mixing of existing snowpack air with the infiltrating

ambient air, but it is sufficient to calculate a lower bound on the air flow $\dot{V}_t$ which is required to dilute ^{222}Rn at a given rate. Also, radioactive decay of ^{222}Rn is ignored in this calculation since the decay constant λ for radon is very small compared to the ventilation decay constant T for cases of interest.

2.6 *Wind-driven air flow in seasonal snowpack*

Turbulent air flow can cause pressure oscillations over a surface. If the snow surface is sufficiently permeable, this "turbulent pumping" can cause ambient air to flow into and exchange with the air below the snow surface. This phenomenon has been observed for radon in soil and SF_6 in snow.(Kraner et al., 1964), (Albert and Shultz, 2002) The magnitude of the pressure oscillations and therefore the exchange rate of ambient and porespace air is proportional to the wind speed, surface roughness and permeability of the substrate.(Albert, 1996a) This wind-driven flow is a component of the total in-pack airflow $\dot{V}_t$ which plays an important role in the radon dilution theory presented in Section 2.5.

Air flow velocity v through a porous medium is driven by a pressure gradient and described by the Darcy equation(Albert, 1996b):

$$v = -\left(\frac{K_i}{\mu}\frac{\partial P}{\partial z}\right) \tag{11}$$

where K_i is the intrinsic permeability of the medium and μ is the viscosity of air. This velocity can be used to determine a volumetric flow rate $\dot{V}$ by determining the area A through which the fluid flowing. This volumetric flow rate is calculated as $\dot{V} = vA$.

2.7 *Natural circulation air flow in seasonal snowpack*

The radon concentration within the snow can also be influenced by natural circulation air flow. Natural circulation is air flow driven by density differences between two adjoining air parcels. The likelihood of this flow occurring is quantified by calculating the dimensionless Rayleigh number, Ra, which compares the the magnitude of the buoyant forces with the viscous forces associated with the fluid and the medium through which it is moving. The Rayleigh number for evaluating natural circulation flow in a porous medium is

$$\mathrm{Ra} = \frac{g\beta(\Delta T)dK_i}{\kappa\nu} \tag{12}$$

where g is gravitational acceleration, β is the thermal expansion coefficient and ΔT is the difference in temperature between the bottom and top layers of fluid.(Powers et al., 1985) A negative value for ΔT implies stable conditions since a system with a cold, dense air parcel beneath a warm parcel will remain static. κ is an effective thermal diffusivity of the fluid-porous medium combination, equal to $k_m/(\rho C_p)_f$, where k_m is the thermal conductivity of the medium and $(\rho C_p)_f$ is the volumetric heat capacity of the fluid.(Lunardini, 1981) ν is the kinematic viscosity of the fluid.(Incropera, 1996)

To estimate the rate of buoyancy-driven airflow, we first calculate the buoyant force F_B on a parcel of air of height l, area A and density ρ which exists inside a large volume of air at density ρ_0:

$$F_B = (\rho_0 - \rho)Alg \tag{13}$$

Since this force acts uniformly over the area A, the pressure gradient $\partial P/\partial z$ created by this parcel is

$$\frac{\partial P}{\partial z} = \frac{F_B}{Al} \tag{14}$$

Finally, this expression for the pressure gradient is used in Eq. 11 to determine the velocity of the parcel through the porous medium. Using this velocity and the snow depth, we can determine the length of time for the parcel to leave the snowpack. Since the volume of the parcel is known, we can determine the volumetric flowrate due to natural circulation as $\dot{V}_{\mathrm{NC}} = V_{\mathrm{parcel}}(v/d)$.

3 MATERIALS AND METHODS

A wide variety of methods were used to test various aspects of the hypothesis posed in Section 1. The concentration of radon in the snow was measured to determine the radon distribution both as a function of position and as a function of time at a fixed position. Sections 3.1, 3.2 and 3.3 explain the various techniques used to measure the activity concentration within the snowpack. The last section details the in-snow solar input and temperature measuring and logging system constructed for this study.

3.1 *Honeywell Professional Radon Monitor*

The Honeywell model A900A Professional Radon Monitor* detects the radiation from radon and its daughters using a silicon alpha particle detector. This device is capable of recording the radon concentration in air on an hourly basis and storing up to 96 such measurements in its memory.

The power supply consisted of two 12V Eveready model 732 lantern batteries connected in series which

*Honeywell International Incorporated, 101 Colombia Road, Morristown, NJ 07962

had adequate capacity to power the detector for roughly two weeks. When fully assembled, the box weighed about 6 kg and placed the center of the detector 24 cm above the bottom of the box.

This detector was deployed by digging a trench in the snow down to ground level, followed by hollowing out a 0.5 m side tunnel with suitable dimensions to accept the detector housing box. The purpose of the side tunnel was to ensure that the detector was located under undisturbed snow. The detector was started on the surface, allowing the operator to verify that it was operating properly, and then placed on the ground at the end of the side tunnel. The side tunnel and trench were then refilled and the detector left to run until its memory capacity was exhausted 96 h later.

3.2 *RAD-7 Radon Instrument*

The RAD-7 radon detector is produced by the Durridge Corporation* and consists of a self-contained alpha spectrometer, counting electronics, air pump and lead-acid battery pack. The only external component is the drying rack, which is placed before the inlet to the detector ensuring that the high voltage silicon detector is not shorted out by overly moist air. The

Figure 2: Flux probe setup for RAD-7 radon ground flux measurements.

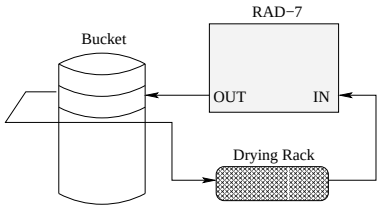

RAD-7 was primarily used with the ground flux probe, illustrated schematically in Fig. 2. The mathematical details for the ground flux measurement are discussed in Section 2.2. The probe consisted of a 9.59 L plastic bucket fitted with inlet and outlet hoses connected to the RAD-7 air inlet and outlet ports via the drying rack. The volume of the remainder of the system external to the bucket, including tubing, drying rack and the active volume of the RAD-7 was 2 L, denoted as $V_{\mathrm{instrument}}$ in Eq. 2.

When connected, this system formed a closed, known volume of air which was simply recycled through the probe and detector by the air pump. Flux measurements require 10 minute counting intervals and many such intervals are needed to observe the radon concentration increase. A typical flux measurement will take over two hours to complete.

*Durridge Corporation, 7 Railroad Avenue, Suite D, Bedford, MA 01730

3.3 *Track-etch radon detectors*

The DRNF RadTrak radon gas detector produced by Landauer† is well suited for outdoor measurements since it is small, lightweight and requires no power source. The detector is a rectangular chip of polycarbonate plastic secured inside of a plastic housing. The polycarbonate chip is damaged by alpha radiation exposure and therefore provides an excellent record of this exposure once the chip is suitably developed and analyzed. Taking the total exposure of the chip and dividing this by the number of days the chip was exposed to the atmosphere yields the average radon concentration over the entire exposure interval.

3.4 *Solar/Temperature (S/T) Instrument*

An important part of studying the dynamics of radon in snow is to measure the changes occurring in the snow itself. Long term measurements of ambient and snow temperatures help to show these changes. Additionally, knowledge of the relative solar input helps to determine when and at what rate snowmelt is occurring. An instrument was designed and constructed to meet the following requirements:

1. Operate for at least one month on 12VDC battery power
2. Sufficient data storage capacity to record one month of half hourly data
3. Three snow temperature probes and one ambient air temperature probe
4. Measure relative solar intensity at one location within snowpack
5. Survive long term burial in alpine snowpack

The Solar/Temperature instrument which resulted from these requirements consisted of three main parts. The first is the battery and interface box, designed to remain near or on the snow surface to provide easy access for the operator to replace batteries and upload stored data without disturbing the rest of the instrument. The solar and temperature probes make up the second part, encompassing all of the various sensors and associated support structures. The final part is the mainboard which contains the microcontroller, voltage regulators, A/D converters and other myriad electronics required for the instrument to operate.

†Landauer Incorporated, 2 Science Road, Glenwood, IL 60425

Figure 3: Main Components of Solar/Temperature Instrument.

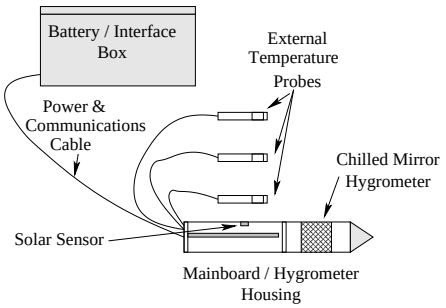

Battery and Interface Box

The battery and interface box is clearly the simplest of the three parts. Containing only a 12VDC battery, an in-line fuse, a main power switch and a female DB-9 connector, this container is designed to protect the battery and the serial computer interface. Since the instrument is designed to upload all stored data on any power interruption, the operator can simply connect a computer running a terminal program, cycle the main power switch and collect the stored data. This feature eliminates the need to use any special program or operating system to retrieve the data.

Instrument Sensors

This instrument uses three separate types of sensors: two different temperature sensors and a solar sensor in the form of a photoresistor. The first type of temperature sensor used is the National Semiconductor* LM335, a solid state device which essentially acts as a Zener diode whose reverse-bias voltage is proportional to temperature. The output voltages of these devices are measured by an analog to digital converter (ADC) located on the mainboard.

The second type of temperature sensor is the DS18B20 produced by Dallas Semiconductor† and is used primarily for external temperature probes. This sensor is also a solid state device, but also has an on-board 12-bit ADC and has the ability to power itself from the communications line, a technique known as a "parasite" power supply. This is especially convenient for external temperature probes since only two wires are required. The devices communicate serially with the microcontroller and can report temperatures at a maximum rate of one measurement per second.

*National Semiconductor Corporation, 2900 Semiconductor Drive, P.O. Box 58090, Santa Clara, CA 95052

†Dallas Semiconductor Corporation, 4401 South Beltwood Parkway, Dallas, TX 75244

The solar sensor consists of photoresistor whose resistance is inversely proportional to the intensity of visible light striking the device. This sensor is mounted in the upper part of the mainboard housing and sealed with transparent tape so that it can have an upward view, yet still maintain the watertightness of the housing. A known voltage, supplied by a Dallas Semiconductor MAX 873 precision voltage supply, is applied to the sensor. The sensor output, the voltage drop across the photoresistor, is measured by an ADC on the mainboard at regular intervals.

The Mainboard

The major components located on the mainboard include a BASIC Stamp 2pe microcontroller by Parallax‡, an MCP3208 ADC produced by Microchip Technology§ and a DS1302 real time clock from Dallas Semiconductor. All components are powered by the 12VDC source in the battery box via a Linear Technology¶ LT1121 12V to 5V DC to DC converter with the exception of the real time clock which operates on a 2 AA cell battery pack located on the bottom of the mainboard. This ensures that the proper time is maintained even in the event of an intermittent main power failure.

The microcontroller is programmable and has 32 kilobytes of EEPROM storage on board where all instrument data is stored. By communicating serially with the ADC, real time clock, temperature sensors and any externally connected computer at the battery box, the microcontroller performs all of the necessary measurement and memory storage and data uploading functions for the instrument. In between measurement periods, the microcontroller shuts down all unnecessary components and then "sleeps" until the next measurement period to conserve battery power.

4 RESULTS AND DISCUSSION

4.1 *Site Description*

Grafton Notch lies on the western border of Maine, separating the Mahoosuc Range on the west from the Baldpate mountains to the northeast. The mountains in this region are high by Maine standards with the summits of Old Speck Mountain at 1274 m and Baldpate Mountain at 1162 m elevation. These mountains support zones of both coniferous and hardwood forest depending on elevation and exposure to the prevailing

‡Parallax Inc., 599 Menlo Drive, Suite 100, Rocklin, CA 95765

§Microchip Technology Inc., 2355 West Chandler Blvd., Chandler, AZ 85224

¶Linear Technology, 1630 McCarthy Blvd., Milpitas, CA 95035

weather. The maximum snow depth observed at this site was 105 cm near the summit of Baldpate Mountain in March 2004.

Table 2: Waypoint Positions and Elevations

	Lat.	Long.	Elev.
160	N 44°35.841″	W 070°55.880″	740 m
161	N 44°36.020″	W 070°54.800″	818 m
162	N 44°36.043″	W 070°54.254″	1074 m
163	N 44°36.002″	W 070°54.634″	908 m
164	N 44°35.376″	W 070°56.865″	466 m
166	N 44°35.603″	W 070°56.599″	480 m

4.2 *Results from Grafton Notch*

Track-etch detectors

Twenty-five track-etch detectors were deployed in Western Maine, the majority of them on the slopes of Baldpate Mountain, from 5 to 29 March 2004. The results are shown in Table 3 on page 7, and show that the thicker and older snow of western Maine prevented ground freezing. Comparing the track-etch data between exposed and protected locations shows evidence for wind-driven airflow through the snowpack. The lowest ground level radon concentration of only 4 pCi L^{-1} was found at waypoint 162, on the western side of Baldpate summit, whereas the highest of over 32 pCi L^{-1} was found at waypoint 161 in a protected col.

Table 3: Grafton Notch track-etch data, 5-29 March 2004.

Location	Depth	Exp.	pCi L^{-1}
160	Bkgd.	24 d	<1.3
160	4 cm	24 d	3.6
160	45 cm	24 d	8.0
160	85 cm	24 d	21.4
160	85 cm	24 d	15.4
161	Bkgd.	24 d	<1.3
161	4 cm	24 d	2.3
161	30 cm	24 d	6.5
161	60 cm	24 d	7.4
161	100 cm	24 d	32.2
162	Bkgd.	24 d	<1.3
162	4 cm	24 d	1.7
162	30 cm	24 d	<1.3
162	60 cm	24 d	3.7
162	104 cm	24 d	4.0
163	Bkgd.	24 d	<1.3
163	4 cm	24 d	<1.3
163	30 cm	24 d	3.2
163	60 cm	24 d	2.9
163	102 cm	24 d	4.1

RAD-7 flux measurements

Several flux measurements were made during the winter of 2004, the data for which are shown in Figs. 4 and 5. Φ_g at waypoint 164 is calculated to be 0.49 pCi m^{-2} s^{-1}. The two data sets for waypoint 166 show a snow surface flux measurement followed by a ground flux measurement at the same location. The calculated snow surface flux Φ_s is 0.17 pCi m^{-2} s^{-1} while Φ_g is 0.64 pCi m^{-2} s^{-1}, the highest flux measured in the study.

Figure 4: Grafton Notch waypoint 164 Ground flux data, 16 March 2004.

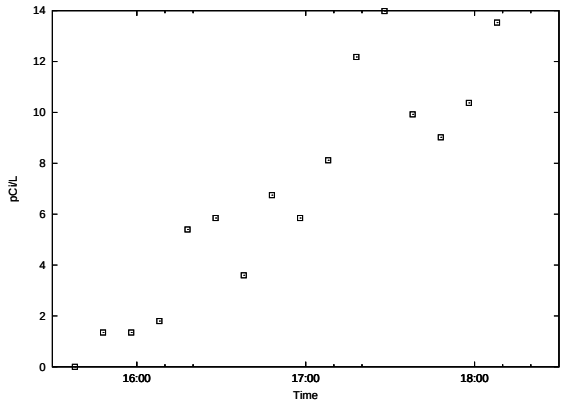

Figure 5: Grafton Notch waypoint 166 Snow surface and Ground flux data, 18 March 2004.

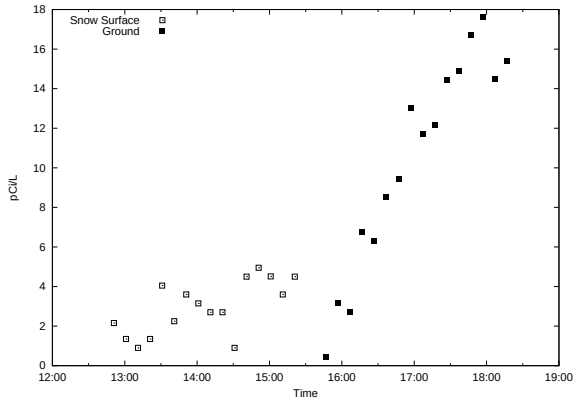

The waypoint 166 data shows that the radon distribution within the snowpack is far from equilibrium at this time, growing into the snow in a fashion similar to that shown in Fig. 8, an exponential distribution. At equilibrium where $\Phi_g = \Phi_s$, the radon concentration will decrease linearly from a high value at ground level to the ambient air value at the snow surface. This equilibrium condition takes several days of quiescent conditions to achieve and was never observed during this study.

Solar/Temperature Instrument Results

The S/T instrument was deployed at waypoint 160 and operated from 17:00, 4 March 2004 through 11:00, 28 March 2004 on a single 12V battery. During this time, it took measurements every 15 minutes despite heavy melting conditions and occasional rainfall during this period. Only the data from 4 to 11 March are shown in Fig. 6 because of the importance of this data for interpretation of the radon concentration data presented in Section 4.2.

Figure 6: Temperature Instrument Data, Waypoint 160, 4-11 March 2004.

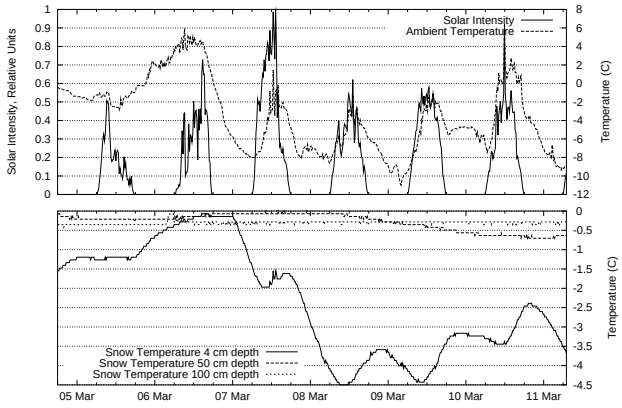

Honeywell radon monitor

The Honeywell radon monitor was deployed at waypoint 160 nearby the S/T instrument and it collected data from 18:00, 4 March until 07:00, 11 March. Interestingly, the largest snowstorm of the month occurred during this time, accumulating several inches between 13:00 and 19:00 on 5 March. The results of the radon measurement and salient weather observations from the Berlin, NH Municipal Airport are plotted in Fig. 7. Ambient temperatures at the measurement site were typically two or three degrees colder than those measured at Berlin, primarily due to the higher elevation of the measurement site. We would expect higher windspeeds at the measurement site for this same reason. The Rayleigh number calculation was performed using the local ΔT measured by the S/T instrument between the snow pack and ambient air.

5 - 6 March 2004

Two prominent peaks in radon concentration occur in the mornings of 5 and 6 March, separated by five hours of very low, near-background levels during the strong winds that accompanied the afternoon snowstorm. A second low radon level period extends for about 24 h between the afternoons of 6 and 7 March, again coincides with the strong winds of a frontal passage. The minimum in-pack air exchange required for the observed -1.3 pCi L^{-1} h^{-1} dilution rate from a maximum of 10 down to 2 pCi L^{-1} is 2×10^{-4} m^3 s^{-1} or about 700 L h^{-1}, a flow easily generated by windspeeds of this magnitude.

Turning now to diffusion theory, we estimate the radon concentration rate during the 5 h period of calm which leads to the peak in radon concentration just before noon on 6 March. This period was modeled by starting with a radon-free snowpack and allowing radon to diffuse into the pack with a constant ground flux boundary condition of $\Phi_g = 0.49$ pCi m^{-2} s^{-1}, the measured ground flux at waypoint 164. Snow porosity was set uniformly to 52%, an appropriate value for ripe snowpack. Fig. 8 shows radon distributions plotted every 30 minutes during this in-growth period. The center of the detector's active volume sits 24 cm above the ground, or 0.76 m depth for the 1 m deep snow at waypoint 160. Here, the diffusion model calculates a

Figure 8: Radon diffusion model applied to 6 Mar 04 radon peak.

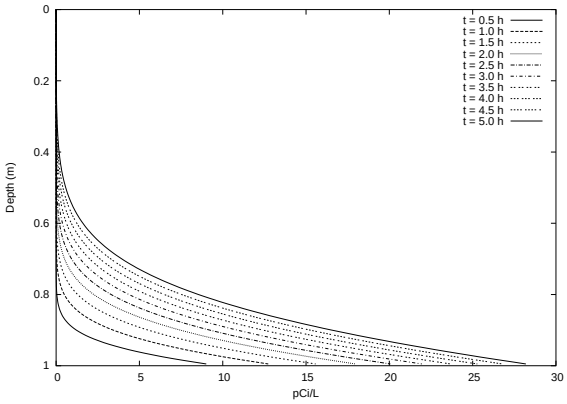

radon concentration of 6.5 pCi L^{-1} at 0.76 m depth, in reasonably good agreement with the measured value of 5.2 pCi L^{-1}, a 25% overestimate. This result also supports setting $\chi = 3$ in Eq. 5.

Note that the Rayleigh number is either very low or negative until the evening of the 7th due to the warm ambient air. Therefore, this period of data is a good example of the effect of wind-driven flow on in-pack radon concentrations with no natural circulation.

7 - 8 March 2004

The next several days have much colder ambient air temperatures and light winds and are interesting because of the very slow build up of radon over time. Radon concentration increases steadily at 0.17 pCi L^{-1}

Figure 7: Meteorological conditions and radon concentration trend, waypoint 160, 4-11 March 2004.

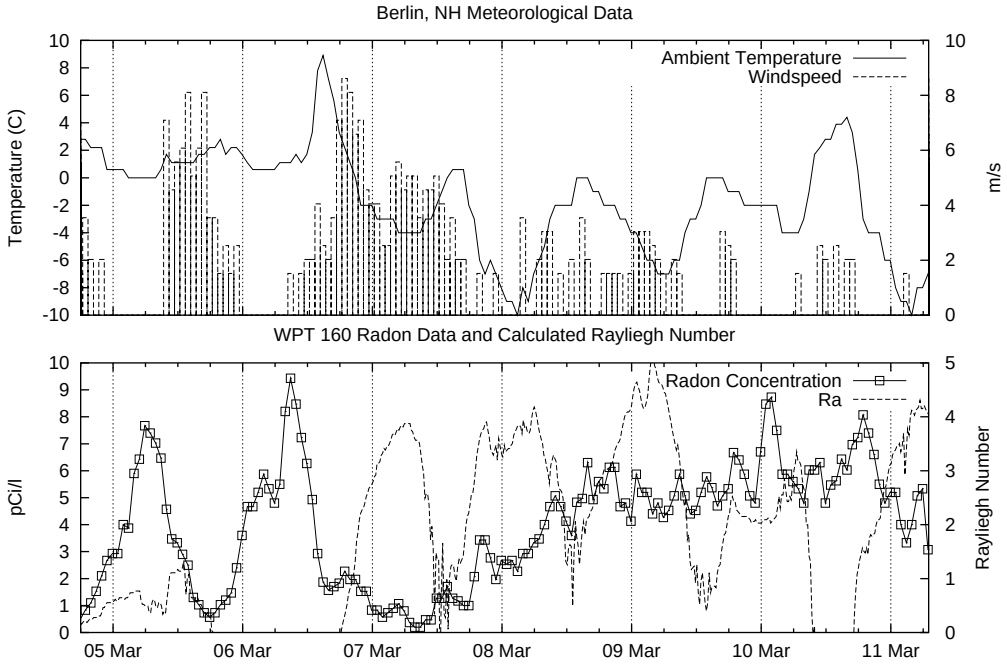

h^{-1} from the morning of 7 March until the evening of 8 March.

The average windspeed during the slow buildup of radon was 2.2 m s^{-1} which would cause a very small flow through the pack, on the order of 50 L h^{-1}. Applying the dilution theory to flowrates of this magnitude, we can see from Eqn. 10 that this flowrate is less than the critical flowrate value of 1.5×10^{-4} m^3 s^{-1} (550 L h^{-1}) where the dilution is slower than the radon input; therefore the radon concentration must increase with time.

We can use Eq. 9 to calculate the minimum flow rate necessary to cause the observed rate of increase. For the conditions in this period of time, a 95 L h^{-1} flowrate is the minimum required to achieve the observed concentration rate of 0.17 pCi L^{-1} h^{-1} during this time period. Comparing this requirement with the average wind-driven flowrate of 50 L h^{-1}, we can see that additional air flow is required. Therefore, we evaluate the likelihood and magnitude of any natural circulation flow during this period.

Rayleigh numbers are quite low for the first 48 h of the measurement period, but with the passage of a cold front during the afternoon of 6 March, the evening values for Ra become significant. For the average Ra of 3.5 calculated for the evening of 7-8 March, we use air densities $\rho_0 = 1.33$ kg m^{-3} and $\rho = 1.32$ kg m^{-3} to calculate a buoyant pressure of 0.098 Pa. Using a permeability range for K_i of 40 to 80×10^{-10} m^2, we calculate a natural circulation flowrate of approximately 82 to 164 L h^{-1}. Combined with the average wind-driven flowrate for this time period, a total flowrate range of 132 to 214 L h^{-1} is calculated, which exceeds the minimum by at least 40%, yet is less than the critical flowrate of 550 L h^{-1}. This is evidence for natural circulation flow during this time period.

9 - 11 March 2004

The remainder of the measurement period is marked by relatively constant radon concentrations of 6 pCi L^{-1}, punctuated by a 9 pCi L^{-1} peak at 01:00, 10 March and a 8 pCi L^{-1} peak at 19:00 of the same day. Both of these events are correlated with periods of combined low windspeed and weak Rayleigh numbers. At the very end of the measurement period, we observe another dilution cycle, this time apparently driven only by natural convection flow with a maximum Ra value of 4.2.

4.3 *Discussion*

In light of the results assembled here, let us revisit the questions posed in the Introduction and evaluate the validity of the hypothesis.

1. Is ^{222}Rn movement driven by heat fluxes and does it therefore migrate with water vapor within the snowpack?

The radon concentration peaks measured at Baldpate early in the morning on 5 and 10 March show that this is not the case, since the maximum heat flux into the snow is experienced in the middle of the day. While it is true that the maximum heat flux out of the snow occurs late in the evenings, the radon concentration minima observed are far more strongly correlated with high winds and high Ra values than they are with the conditions associated with large heat transfers out of the snowpack such as clear skies and low overnight temperatures. Radon should not be used to trace water vapor transport in snow.

2. Does meltwater formation in the upper layers of the snowpack in the effectively "seal" the surface of the snow, thus preventing the escape of ^{222}Rn from the snow?

   The strongest melting conditions observed during the Baldpate measurement period occur on the afternoon of 6 March, which coincides with the strongest observed radon dilution rate of the entire study. This evidence, coupled with the `SNTHERM.89` simulation and diffusion theory which predict a minimal change in snow porosity and Φ_s, show that meltwater does not block the porespace of the snow in any significant fashion.

3. Are wind-driven and natural circulation air flows significant in terms of their diluting effect on the ^{222}Rn concentration within the snowpack?

   Wind-driven airflow is the dominant factor controlling radon concentration in seasonal snowpack. The data shows a very strong correlation between high wind speed and rapid radon dilution. During periods of low wind speed, natural circulation flow seems to have a noticeable effect on radon concentration rate. From this data, it seems that natural circulation probably does not occur in this snowpack for Rayleigh numbers less than 3.

5 CONCLUSION

The theory, radon measurement methods and measurement results obtained from a research site located in Western Maine have been presented. Results show that wind-driven flow is the dominating factor affecting the radon distribution followed by natural circulation airflow. This is an important result for future heat transfer studies of seasonal snowpack since radon dynamics can be used to measure the amount of air flow within the snowpack.

REFERENCES

Albert, M. and Shultz, E.: 2002, Snow and Firn Properties and Air-Snow Transport Processes at Summit, Greenland, Atmospheric Environment 36, 2789

Albert, M. R.: 1996a, in Chemical Exchange Between the Atmosphere and Polar Snow, No. 43 in Nato ASI, pp 561–565, Spring-Verlag

Albert, M. R.: 1996b, Modeling heat, mass and species transport in polar firn, Annals of Glaciology 23, 138

Baum, E. M. et al. (eds.): 2002, Chart of the Nuclides, Knolls Atomic Power Laboratory, sixteenth edition

Boas, M. L.: 1983, Mathematical Methods in the Physical Sciences, John Wiley and Sons, second edition

Carroll, T.: 2001, Airborne Gamma Radiation Snow Survey Program Users Guide, National Operational Hydrologic Remote Sensing Center, NOAA, 5.0 edition

Cember, H.: 1992, Introduction to Health Physics, McGraw-Hill, second edition

Gunderson, L. Schumann, R.: 1993, in Geologic Radon Potential of EPA Region 1, open file report 93-292-a 4, pp 83–122, U.S. Geological Survey

Incropera, Frank P. DeWitt, D. P.: 1996, Introduction to Heat Transfer, John Wiley and Sons, third edition

Jordan, R.: 1991, A One-Dimensional Temperature Model for a Snow Cover, Technical Documentation for SNTHERM.89, Technical report, Cold Regions Research and Engineering Laboratory, 72 Lyme Road, Hanover, NH 03755

Kraner, H. W. et al.: 1964, in The Natural Radiation Environment, Chapt. 10, pp 191–215, University of Chicago Press

Lockhart, L. B.: 1964, in The Natural Radiation Environment, Chapt. 18, pp 331–344, University of Chicago Press

Lunardini, V. L.: 1981, Heat Transfer In Cold Climates, Van Nostrand Reinhold

Powers, D. et al.: 1985, Theory of Natural Convection in Snow, Journal of Geophysical Research 90(D6), 10641

Tanner, A. B.: 1964, in The Natural Radiation Environment, Chapt. 9, pp 161–181, University of Chicago Press